Wind and Structures, *Vol. 19, No. 4 (2014) 389-404*
DOI: http://dx.doi.org/10.12989/was.2014.19.4.389

Flow control downstream of a circular cylinder by a permeable cylinder in deep water

Bengi Gozmen[1] and Huseyin Akilli*[2]

[1]*Department of Mechanical Engineering, Uşak University, 1 Eylül Kampüsü, 64200, Uşak, Turkey*
[2]*Department of Mechanical Engineering, Cukurova University, 01330, Yüreğir, Adana, Turkey*

(Received August 20, 2013, Revised July 4, 2014, Accepted July 20, 2014)

Abstract. The flow characteristics of a circular cylinder surrounded by an outer permeable cylinder were experimentally investigated using Particle Image Velocimetry Technique in deep water flow. In order to consider the effects of diameter and porosity of the outer cylinder on flow structures of the inner cylinder, five different outer cylinder diameters (D=37.5, 52.5, 60, 75 and 90 mm) and eight different porosities (β= 0.4, 0.5, 0.6, 0.65, 0.7, 0.75, 0.8 and 0.85) were selected. During the experiments, the diameter of inner cylinder was kept constant as d=30 mm. The depth-averaged free-stream velocity was adjusted as U=0.156 m/s, which corresponds to the Reynolds number of Re=5000 based on the inner cylinder diameter. It has been concluded that both the outer permeable cylinder diameter and the porosity have important influences on the attenuation of vortex shedding in the wake region. The presence of outer permeable cylinder decreases the magnitude of Reynolds shear stress and turbulent kinetic energy compared to the bare cylinder case. Moreover, the spectral analysis of vortex shedding frequency has revealed that the dominant frequency of vortex shedding downstream of the cylinder arrangement also reduces substantially due to the weakened Karman shear layer instability.

Keywords: passive control; PIV; circular cylinder; vortex shedding

1. Introduction

The flow around bluff bodies has been a subject of interest to engineers for many years due to its use in numerous engineering applications in particular to the wind and ocean engineering. Despite the fact that the bluff body has a simple geometry, the wake of the bluff body has a complex structure and it contains the interaction of three shear layers: a boundary layer, a separating free shear layer, and a wake (Williamson 1996). Depending on these effects, two dimensional (2-D) or three dimensional (3-D) vortical instabilities (Thompson *et al*. 1996) are obtained in wakes of bluff bodies. Our focus in this study is on 2-D wake phenomena. The shedding of vortices in the near wake leads to large fluctuating pressure forces in a direction transverse to the flow and causes structural vibrations, enhanced mixing, and acoustic noise. Many works on wake flow have been conducted on control the undesired effects of vortex shedding (Gad El. Hak 2000, Choi *et al*. 2008) with active and passive means. Active control methods have been

∗Corresponding author, Professor, E-mail: hakilli@cu.edu.tr
[a] Ph.D., E-mail: bengi.gozmen@usak.edu.tr

http://www.techno-press.org/?journal=was&subpage=8 ISSN: 1226-6116 (Print), 1598-6225 (Online)

defined as input of external energy into the flow field. Rotational oscillaratory (Lee and Lee 2008, Doll *et al*. 2008), suction and blowing (Li *et al*. 2003, Fransson *et al*. 2004, Min and Choi 1999), syntetic jet (Akansu and Fırat 2010, Feng and Wang 2010), piezo actuators (Cattafesta *et al*. 2001) etc. are applied to suppress the unsteady flow structure of bluff body.

The passive control technique which is energy free and easier to implement controls the wake region by modifying the shape of bluff body or by attaching additional devices into the flow region. For example, control cylinder, trip wires, o-rings, splitter plate, and porous - permeable devices come under passive control techniques. Lee *et al*. (2004) studied on the effects of a small control rod on drag characteristics and wake structure behind the cylinder. They placed a small control rod upstream of the cylinder. They reported that the drag coefficient and wake structure changed significantly depending on pitch distance L between the main cylinder and control rod. They obtained a critical pitch distance L_c, at which vortices start to shed from the control cylinder. Wang *et al*. (2006) investigated effects of a rod on the drag reduction around a circular cylinder. They observed that the existence of the control rod was effective on drag and lift reduction. Kuo and Chen (2009) placed symmetrically two small control cylinders along the separating shear layers at various stream locations at Re=80. They revealed that fluctuating lift on the main cylinder reduced 70-80% and the total drag reduction of all the cylinders was about 5% when the control cylinders were placed in the range of $0.8 \leq X_c/D \leq 3.0$. The flow characteristics of the wakes behind circular cylinders fitted with o-rings were investigated by Lim and Lee (2004). They showed that the vortex formation region behind the cylinder fitted with o-rings extended, and drag force acting on the cylinder decreased at high Reynolds numbers. Nakamura and Igarshi (2008) achieved the suppression of vortex shedding by attaching cylindrical rings around the cylinder. They reduced drag and fluctuating forces. The using of rings reduced the drag force by 15% for $Re_d \geq 20\,000$ due to the formation of separation bubbles on both sides of the ring, which causes to pressure recovery on the rear of the ring. Ekmekci and Rockwell (2010) investigated the effect of a wire which was attached on the outer surface and parallel to span of a stationary circular cylinder at a range of angular positions from $\theta = 40°$ to 120°. They revealed that the surface wire disturbed only one of the shear layers. This disturbance caused important global consequences over the whole wake. They defined two critical angles effective on near-wake structure. At one critical angle, substantial extension occurred and at the other critical angle, significant contraction of the time-averaged near-wake bubble was observed. Among the passive control methods, the splitter plate has been known one of the most successful passive control methods to control the vortex shedding downstream of the cylinder. Several splitter plate studies have been performed for a few decades. Gerrard (1966), one of the earlier researchers studying on splitter plate, measured the frequency of vortex shedding behind a cylinder with an attached splitter plate. The results of his study showed that the St decreased as the length of the plate increased. Unal and Rockwell (1988) carried out experiments on flow over a circular cylinder with a splitter plate in the Re range of $140<Re<3600$. They divided the flow patterns into two separate regions: pre-vortex formation regime and post-vortex formation regime. While the large-scale vortices upstream of the plate's tip appeared in the post-vortex formation regimes, it disappeared in the pre-vortex formation regime. Nakamura (1996) investigated the vortex shedding from several bluff bodies attached with a splitter plate. The experiments were performed for different Reynolds numbers (between 300 and 5000). It was deduced that the characteristics of vortex shedding changed from Von Karman vortex shedding into impinging shear layer instability by the splitter plate. The thickness effects of the splitter plate on the vortex shedding downstream of a circular cylinder was studied experimentally by Akilli *et al*. (2005). They proved that the change in the thickness of the splitter plate did not have any

considerable effect on the flow structure and the splitter plate had influence on the suppression of vortex shedding for the gap ratio between 0 and 1.75D. Moreover, Akilli *et al*. (2008) focused on the effect of the splitter plate length. They indicated that it had a significant effect on the flow structure, and the length of L/D=1.2 was determined as the critical length in terms of controlling the flow. Yucel *et al*. (2010) studied on the effect of a detached downstream plate on the near wake of a circular cylinder. The experiments were carried out for five different horizontal (G) and seven different vertical (Z) locations between the cylinder and the plate. They observed variations in vortex shedding as a function of vertical and horizontal distances between the body and the plate. Gozmen *et al*. (2013) investigated the effects of splitter plates having different heights and lengths located in the wake region of the circular cylinder in shallow water. They obtained that flow structures changed significantly with height and length ratios of the splitter plates in shallow water. The wake region downstream of the cylinder was elongated along the streamwise direction with increasing the plate length and depth. The case of h_p/h_w=0.75 for L/D=2 was the most effective case on the control of vortex shedding.

Another method of passive control technique is the usage of porous and permeable devices in order to control the flow around bluff bodies. Sobera *et al*. (2006) investigated flow structure at subcritical Reynolds number (Re=3900) around a circular cylinder surrounded by porous layer. They found that the flow in the space between the porous layer and the solid cylinder was laminar and periodic and the frequency of flow was locked to the Strouhal frequency of vortex shedding in wake region. Bruneau and Mortazavi (2006) focused on the control of the flow around a fixed cylinder using a porous layer between the obstacle and the fluid. They showed that the porous layer reduced the shear effects in the boundary layer and change the structure of vortex shedding. Moreover, the Cl_{rms} for the higher value of the Reynolds number close to natural flow conditions decreased by about 72%. Bhattacharrya *et al*. (2006) studied on flow structure around and through a porous cylinder. They revealed that the flow field was steady for the range of Reynolds number ($1 \leq Re \leq 40$) and the drag force decreased monotonically while the Reynolds number was increasing and the Da was decreasing. Bhattacharyya and Singh (2011) performed a numerical study on the laminar vortex shedding and wake flow behind a porous-wrapped solid circular cylinder. They indicated that inclusion of a porous wrapper reduced the strength of the separated shear layers. By porous wrapper, the pressure drop and skin friction which cause a reduction in drag compared with a solid cylinder were decreased. In addition, when a thin porous wrapper ($e_p<1$) was used, the wake structure of the porous cylinder became similar to that of a wake of a solid cylinder. Flow structure around a cylinder surrounded by a permeable cylinder in shallow water was investigated experimentally by Ozkan *et al*. (2012). They observed that both porosity and outer cylinder diameters had significant effects on controlling the wake region downstream of the circular cylinder. The peak values of turbulent statistics, like turbulent kinetic energy (TKE) and Reynolds stresses were diminished considerably by the outer permeable cylinder. Kleissl and Georgakis (2011) researched the effects of bridge cable shape and surface on the control of wind-induced vibrations. They used four different cable shapes: a circular cylinder, a shrouded cylinder, a wavy, and a facetted cylinder to compare with each other. They revealed that the effect of shrouded cylinder on the flow depends on Reynolds number slightly. And the shrouded cylinder significantly reduced the vortex-induced oscillating lift forces. The drag coefficient was measured as slightly above 1.0.

It is possible to use a permeable cylinder as a control device in order to prevent the harmful effects of vortex shedding on various engineering applications such as high-rise chimneys, bridge piers and risers in off-shore engineering etc. For this reason, this investigation aims to elucidate the

effect of permeable cylinder placed around a circular one that has a diameter of 30 mm in deep water. The effect of porosity β and the ratio of the diameter of outer permeable cylinder to the inner cylinder D/d on the flow characteristics have been focused on. In doing that, eight different porosities and five different outer cylinder diameters were selected.

2. Experimental method and apparatus

Experiments were conducted in a 8,000 mm x1,000 mm x750 mm circulating open water channel located at Fluid Mechanics Laboratory of Mechanical Engineering Department of Çukurova University. The PIV technique was applied to calculate the instantaneous and time-averaged velocity vector fields downstream of a circular cylinder with a diameter of d=30 mm in order to understand the effect of outer permeable cylinder which is concentrically placed around the inner cylinder. The side view of experimental system and the placement of inner - outer permeable cylinders were indicated in Fig. 1a. The outer permeable cylinder was made of a chrome-nickel wire mesh while the inner cylinder is made of transparent plexiglass material. In the current study, porosity is defined as the ratio of gap area on the body to the whole body surface area. And the porosites of the outer permeable cylinder were selected as β= 0.4, 0.5, 0.6, 0.65, 0.7, 0.75, 0.8 and 0.85. To reveal the effect of the diameter ratios, five different diameters of outer permeable cylinder (D=37.5, 52.5, 60, 75, and 90 mm) were used. The choice of these parameters is based on the studies of Pinar *et al*. (2011) and Ozkan *et al*. (2012). All the parameters mentioned in this study were shown in Fig. 1(b). The total depth of the water channel was set at 560 mm. All experiments were performed above a platform and the couple of the inner and outer cylinder was placed at 1750 mm from the leading edge of the platform in order to obtain a fully developed boundary layer. The water height between the base of the platform and the free surface (h_w) was adjusted to 340 mm. The flow measurement was carried out at the mid-depth of the water between the base of the platform and the free surface (h_L). The geometric blockage ratio of the inner cylinder was 3%. When the diameter of the permeable outer cylinder is taken into consideration, the geometric blockage ratio rises to 9%. The free-stream velocity was U_∞= 156 mm/s, yielding Reynolds number based on the inner cylinder diameter of Re=5000. This desired velocity was adjusted by a centrifugal pump with a speed control unit.

Quantative flow images are acquired and processed by Dantec Dynamic PIV system and Flow Manager Software. The illumination laser light sheet was generated by a pair of double-pulsed Nd:yag laser units each with a maximum energy output of 120mJ at 532-nm wavelength. The thickness of the laser sheet illuminating the measurement plane was approximately 2 mm. The flow fields were captured using a 8 bit cross correlation CCD camera with a resolution of 1600x1200 pixels, equipped with a Nikon AF micro 60 f/2.8D lens. The camera and laser pulses were triggered with correct sequence and timing using a synchronizer. In the image processing, the images are interrogated using a double frame, cross-correlation technique with a window size of 32x32 pixels and a 50% overlapping. The time interval between the pulses was 1.5 ms. This time interval provides approximately a maximum particle displacement of 10 pixels. A total of 3844 (62x62) velocity vectors were captured for an instantaneous velocity field at a rate of 15 frames per second. For all experiments, two flow fields one after the other were taken to provide a better observation of the flow data in the wake of the inner cylinder. The size of measurement field was set to 200 mm x 200 mm in physical size. The water was seeded by silver-coated hollow glass

spheres of 12 μm mean diameter and the density of the particles was 1100 kg/m^3. The particles track the flow corresponding nondimensional Stokes Number 1.83x10^{-4} (Raffel *et al*. 1998). The statistical properties of the flow field were adequately assessed using 350 instantaneous images. Spurous velocity vectors were identified with the local median-filter technique and they were replaced by interpolated vectors which were calculated by means of a bilinear least square fit technique between neigbouring vectors. In velocity measurement, the seeding particle size, particle overlap, non-uniform particle distribution and the size of interrogation window are the effective parameters on uncertainty. In this study, the uncertainty in the vector field at 95% confidence interval was calculated as 2%.

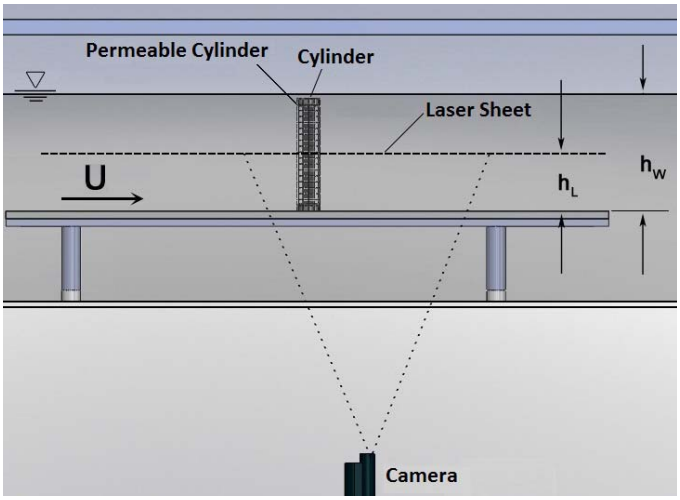

(a)

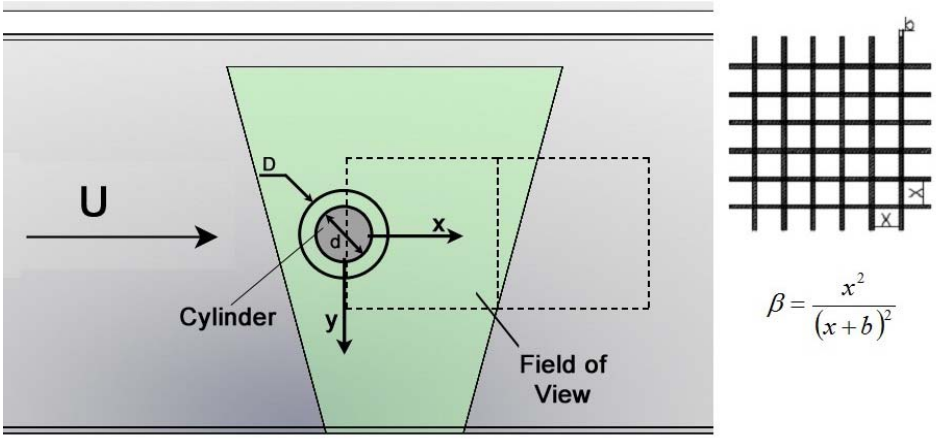

(b)

Fig. 1 (a) Side view of experimental system and the placement of inner cylinder - outer permeable cylinder and (b) A sketch of wire mesh and defination of the parameters: cylinder diameter d, permeable cylinder diameter D, wire diameter b, dispacement between two wires X, porosity β, and free-stream velocity U

3. Results and discussion

3.1 Time-averaged flow patterns

To reveal the effects of porosity and diameter ratio, Reynolds shear stress contours of various porosities (β= 0.4, 0.6, 0.7 and 0.8) are presented in Figs. 2(a) -2(c) for diameter ratio of D/d=1.25, 2, and 3, respectively. The Reynolds shear stress has been normalized by the square root of the depth-averaged free-stream velocity. The minimum and incremental values of Reynolds shear stress are selected as ±0.002 and 0.002, respectively. The solid lines show positive (counter-clockwise) contours of Reynolds shear stress while the dashed lines indicate the negative (clockwise) contours. Fig. 2(a) demonstrates the contours of Reynolds shear stress for the diameter ratio of D/d=1.25. The gap between the inner cylinder and the outer permeable cylinder is so narrow that two cylinders act as a whole cylinder which has a diameter of 37.5 mm. Therefore, the peak values of Reynolds shear stress for all porosities in Fig. 2(a) are higher than that of the bare cylinder case which has a value of 0.0405. On the other hand, the location of peak concentration of Reynolds shear stress alters as porosity increases. The peak concentration occurs at a location of x/D=1.5 for bare cylinder; however, the location of peak concentration moves approximately x/D=3.7 for the porosities 0.4≤ β ≤0.7. For β=0.8, since the open area on the surface of the outer cylinder is too large, the outer permeable cylinder becomes less effective in terms of the location of peak Reynolds shear stress. Therefore, the location of peak Reynolds shear stress, x/D=1.95, gets closer to the base of the outer permeable cylinder. However, the magnitude of peak Reynolds Stress decreases at this porosity.

Fig. 2(b) illustrates the contours of Reynolds shear stress for the diameter ratio D/d=2.0. For the porosities of 0.4≤ β ≤0.7, the magnitude of Reynolds shear stress gradually decreases with the increase in the porosity due to the prevention of the interaction of the shear layers at the outer cylinder. As the peak of Reynolds shear stress for β=0.4 locates at the end of the first field of view, the peaks of $< u'v' >$ for β=0.6 and 0.7 situate in the second field of view. The maximum reduction in the peak value of Reynolds shear stress which is approximately 55 % of that of the bare cylinder case is obtained at the porosity of β=0.7. In terms of β=0.8, the magnitude of Reynolds shear stress increases slightly compared to the porosity of β=0.7 in the first field of view. In contrary, the magnitude of $< u'v' >$ reduces to 0.0143 in the second field of view. This means that the permeable cylinder having the porosity of β=0.8 loses its effect on the attenuation of vortex shedding. Furthermore, the concentration of Reynolds shear stress shrinks in the cross-stream direction as the porosity increases. For β=0.7 and 0.8, an increase in Reynolds shear stress concentration occurs just downstream of the cylinder arrangement as a result of the increase in the open area on the surface of the outer cylinder. It can be concluded that the outer cylinder has little effect on the suppression of vortex shedding, so unsteady flow structure occurs in the region between the inner and outer cylinders.

The outer permeable cylinder having the diameter of 3d suppresses significantly the vortex shedding downstream of the outer cylinder as can be seen from the Fig. 2(c). For this diameter ratio, the reduction in the Reynolds shear stress reaches to 52 and 73% of that of the bare cylinder case for β=0.6 and 0.7, respectively.The porosity of β=0.7 for this diameter ratio is most effective case on the attenuation of vortex shedding downstream of the cylinder arrangement. No distinct large scale vortices can be observed in the downstream of the cylinder arrangement. For β=0.8, the peak value of Reynolds shear stress forms very close to the base of the inner cylinder-outer permeable cylinder arrangement as the peak magnitude occurs in the second field of view for the

remaining porosity values. In addition, the magnitude of $< u'v' >$ increases compared to the case of β=0.7.

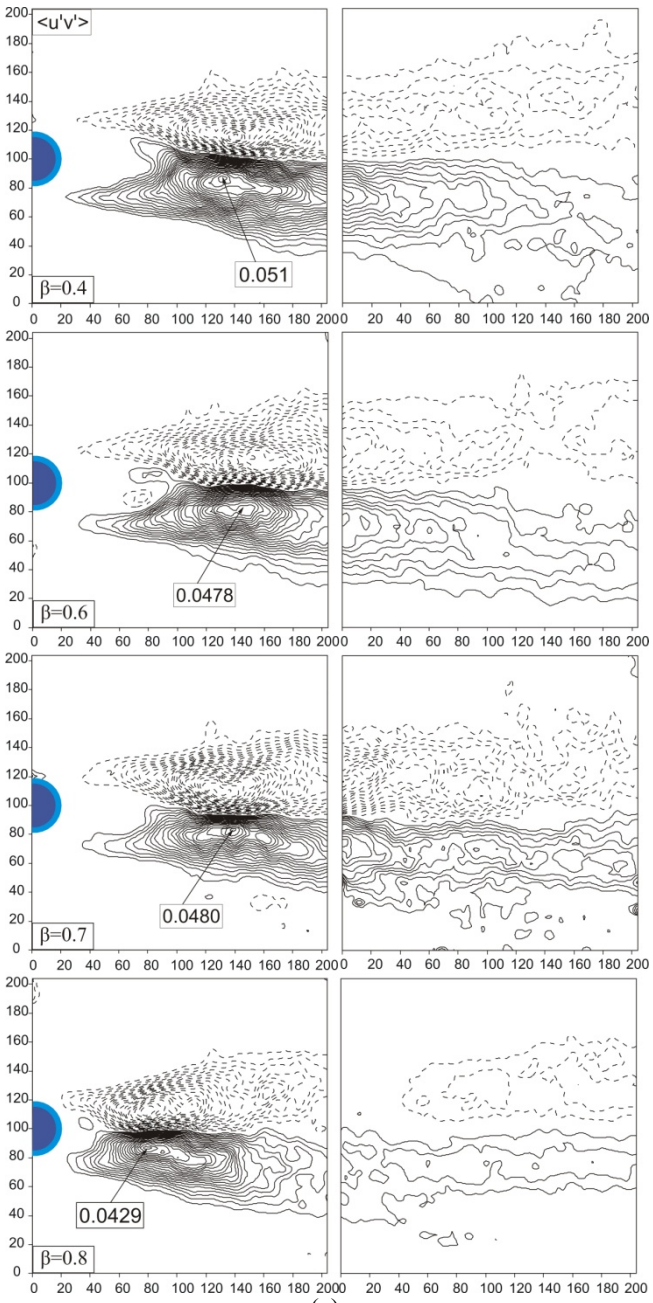

(a)

Continued-

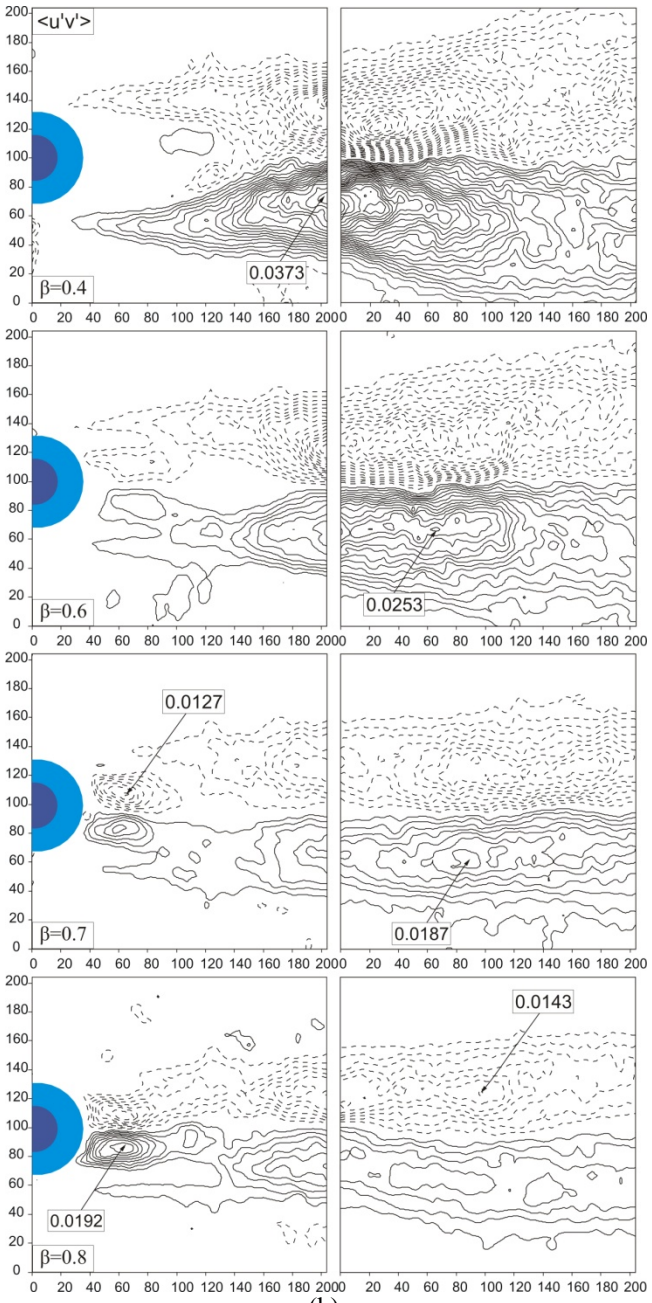

(b)

Continued-

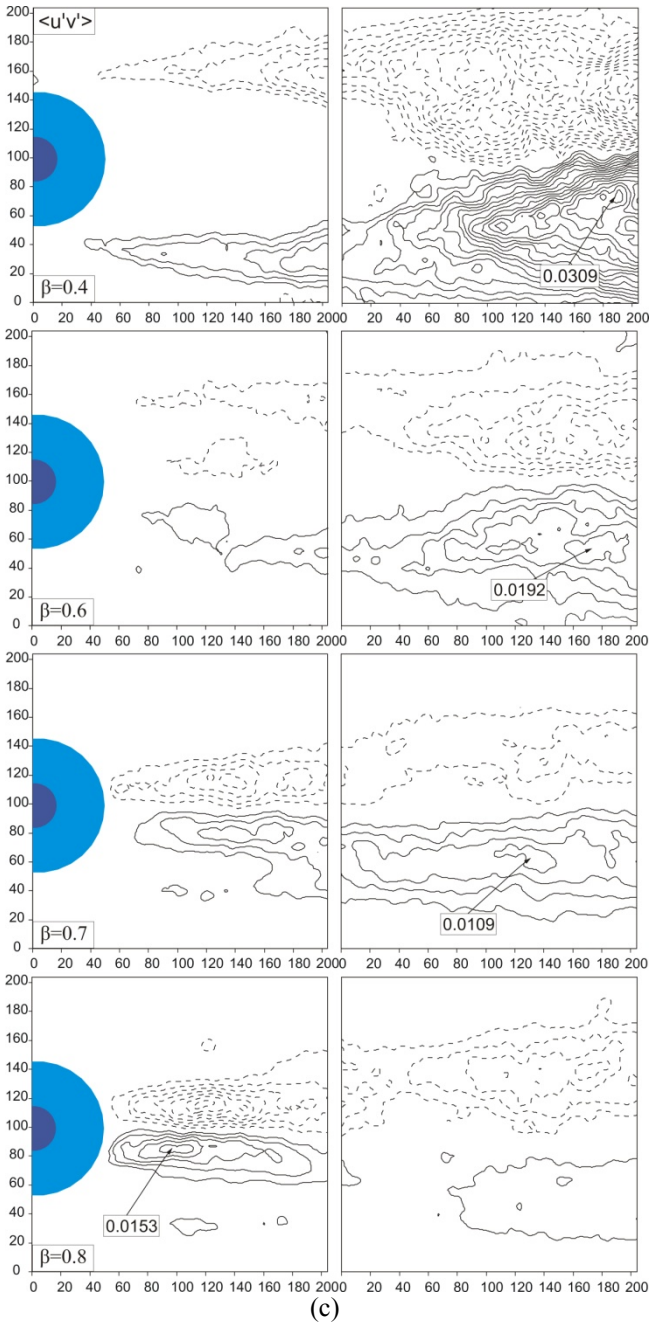

Fig. 2 (a) Contours of Reynolds shear stress for the diameter ratio D/d=1.25, (b) Contours of Reynolds shear stress for the diameter ratio D/d=2.0 (c) Contours of Reynolds shear stress for the diameter ratio D/d=3.0

Contours of the time-averaged streamwise velocity <u>/U for the bare cylinder case and the cases of cylinder arrangements of various outer cylinder diameter ratios for the porosity of β=0.7 are given in Fig. 3. The dashed lines present negative values of <u>/U, whereas the solid lines indicate positive values. The substantial region of reverse flow is evident for the bare cylinder case and for the case of D/d=1.25. The streamwise pocket length of negative <u>/U indicates that when the outer permeable cylinder having the diameter of 37.5 mm is placed around the inner cylinder, the pocket length of negative <u>/U shows an increase in comparison to the bare cylinder case. For these cases, stagnation points, S, which are shown by black dots occur at the locations of 1.46d and 2.06d from the base of the cylinder arrangement, respectively. It is interesting to see that when the diameter ratio increases to a value of D/d=2, reverse flow region disappears instantly. For the cases of D/d=2 and 3, the presence of outer permeable cylinder eliminates the reverse flow as a consequence of the momentum transfer from the holes of the outer cylinder into the wake region.

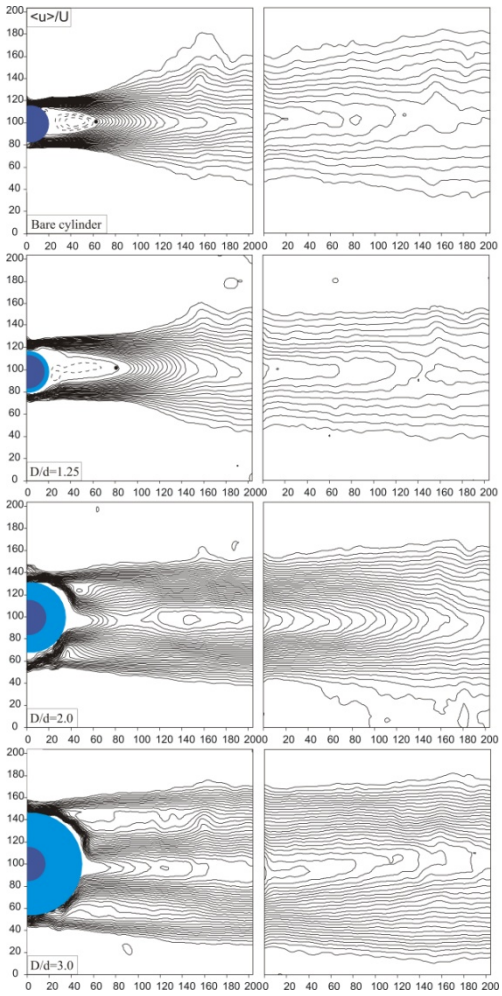

Fig. 3 Contour patterns of time-averaged streamwise velocity <u>/U for bare cylinder and the case of β=0.7 of various diameter ratios D/d. Minimum and incremental values are as follows: $|\langle u\rangle/U|_{min}$= 0.005 and Δ[<u>/U]= 0.005

The shear layers extend symmetrically along the streamwise direction according to the centerline of the cylinders on account of the fact that the annular region between the inner cylinder-outer permeable cylinder enlarges and the significant flow mass can penetrate into the base region of the outer cylinder. Furthermore, an expected observation is the enlargement of wake region in the spanwise direction as the value of D/d increases as a result of the increase in outer cylinder diameter.

Fig. 4 depicts the variation of the time-averaged streamwise velocity component <u>/U along the centerline of the cylinder arrangement for different D/d ratios with the porosity of β=0.7. Here, x/d=0 indicates the base of the outer permeable cylinder. For the bare cylinder case, the occurrance of reverse flow is seen obviously and it continues until the location of x/d=1.5. After this location, the <u>/U increases rapidly. This observation is also in accord with the previous study performed by Ozgoren *et al*. (2011). By the case of D/d=1.25, the magnitude of reverse flow decreases significantly. Moreover, the pocket of negative <u>/U extends along the streamwise direction as seen in Fig. 3. The diameter ratios of D/d=2 and 3 show similar trend with each other. There is no detectable reverse flow region downstream of the cylinder arrangement. The permeable cylinder completely eliminates the reverse flow downstream of the cylinder arrangement. The difference between the time-averaged streamwise velocity <u>/U at the base of the outer cylinder and the <u>/U at the end of the flow field diminishes compared to the cases of bare cylinder and D/d=1.25 due to the fact that the momentum transfer from the free-stream region is prevented by the outer permeable cylinder. Consequently, it can be deduced that as the diameter ratio increases, the effect of the unsteady vortical flow structure resulting in the high velocity difference is reduced significantly.

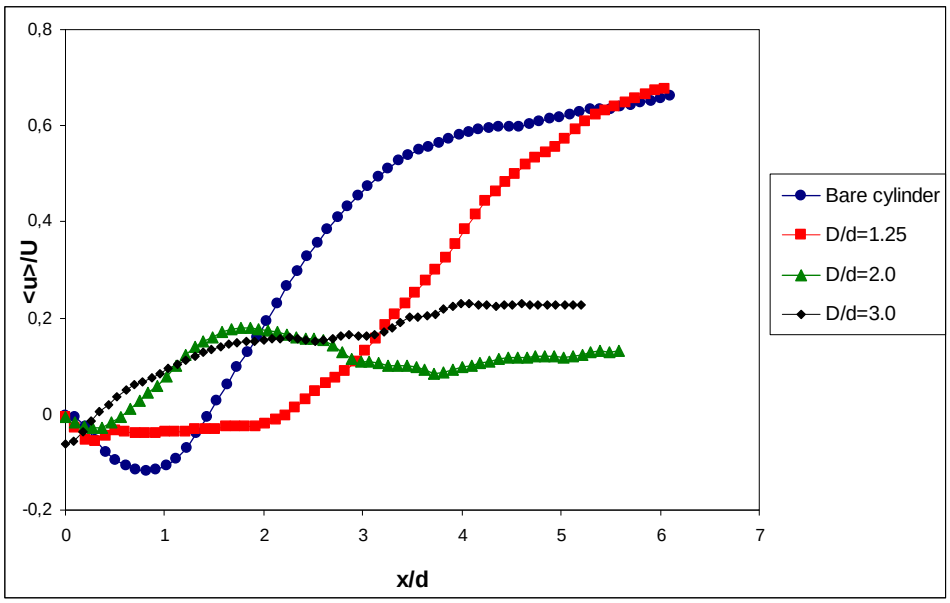

Fig. 4 Variation of the time-averaged streamwise velocity component <u>/U along the centerline of the cylinder arrangement

The variation of peak value of turbulent kinetic energy as a function of porosity is given in Fig. 5 to explore the effect of diameter ratio and porosity. As a general trend, it is evident from the figure that increasing diameter ratio results in a decrease in the peak value of TKE. This means that the occurrence of large scale vortices which transfer momentum from the free-stream flow into the wake is suppressed by the outer permeable cylinder. Besides, the peak values of TKE for $D/d \geq 1.75$ cases attenuate as the porosity increases. However, the peak values of TKE for $\beta=0.8$ and 0.85 cases slightly rise compared to $\beta=0.75$. This is due to the unsteady vortical flow structure inside the annular region between the inner and outer permeable cylinder. As the peak value of TKE for the bare cylinder case is 0.138, this value reduces to 70 % of that of the bare cylinder at most and this reduction is obtained from the case of $\beta=0.7$ for the diameter ratio of $D/d=3$. Moreover, this reduction might be a sign of drag reduction as in the study of Lee and Ko (2009). They noticed that as the turbulent statistics obtained from the PIV decrease, the reduction of drag also shows an increase. Similar trends of $D/d=2$, 2.5 and 3 are evident in Fig. 5 except for the differences in the magnitude, while the case of $D/d=1.25$ shows completely different trend from other diameter ratios. The magnitudes of TKE for all porosities are higher than that of the bare cylinder case since the inner and outer permeable cylinder combination behaves like a solid cylinder having a larger diameter compared to the bare cylinder. The peak values of TKE vary between 0.16 and 0.18 for different porosities.

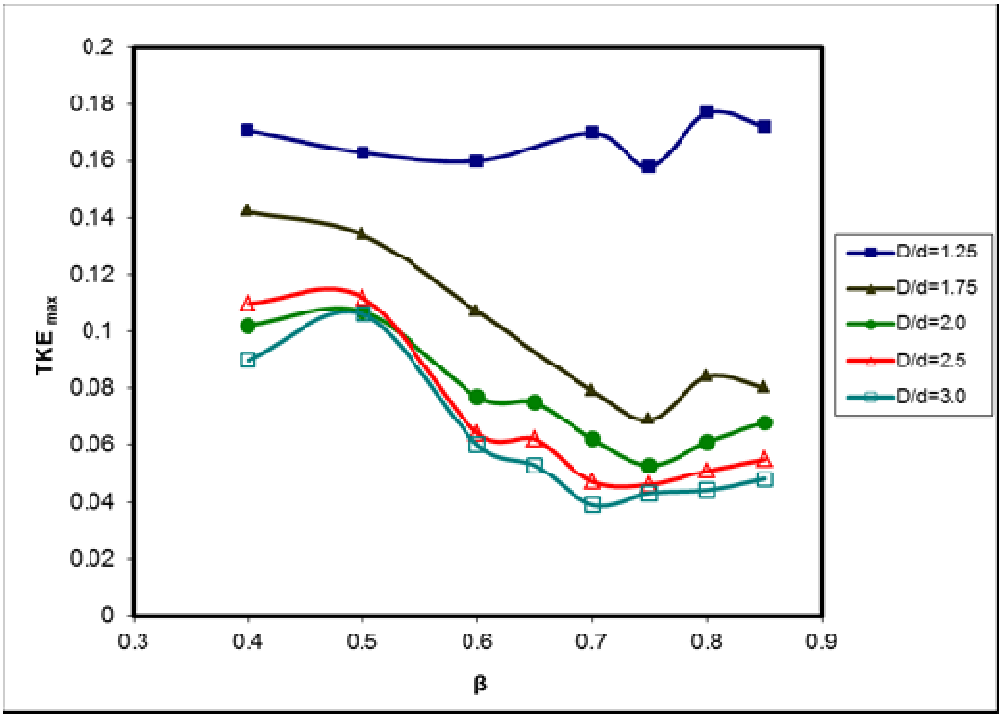

Fig. 5 Variation of peak value of turbulent kinetic energy as a function of porosity for all diameter ratios

3.2 Spectral analysis and calculation of vortex shedding frequency

Fig. 6 depicts spectra of the streamwise component of velocity (u) at a constant location for bare cylinder case and for control cases of β=0.7 for various diameter ratios. The dominant frequencies (f) are obtained from the power spectra of PIV data in the first field of view. This figure clearly points out that the outer permeable cylinder has significant influence on the attenuation of unsteady flow structure. A dominant peak is obtained at f=0.91 Hz for the bare cylinder case. Different dominant frequencies are obtained for each diameter ratio with the presence of outer cylinder. The frequency of unsteady flow decreases gradually as the diameter ratio D/d increases. Dominant frequency occurs at f=0.59 Hz for D/d=2.0, while it occurs (centers) at f=0.32 Hz for D/d=2.0 which is approximately three times smaller than that of the bare cylinder case, confirming to weakened vortex shedding and attenuated forces. Moreover, the amplitude of spectral peak progressively diminishes with increasing diameter ratio. The results obtained from this figure are coincided with the results of turbulent statistics. Namely, TKE and Reynolds shear stress downstream of cylinder arrangement decrease with the increase in the diameter ratio D/d.

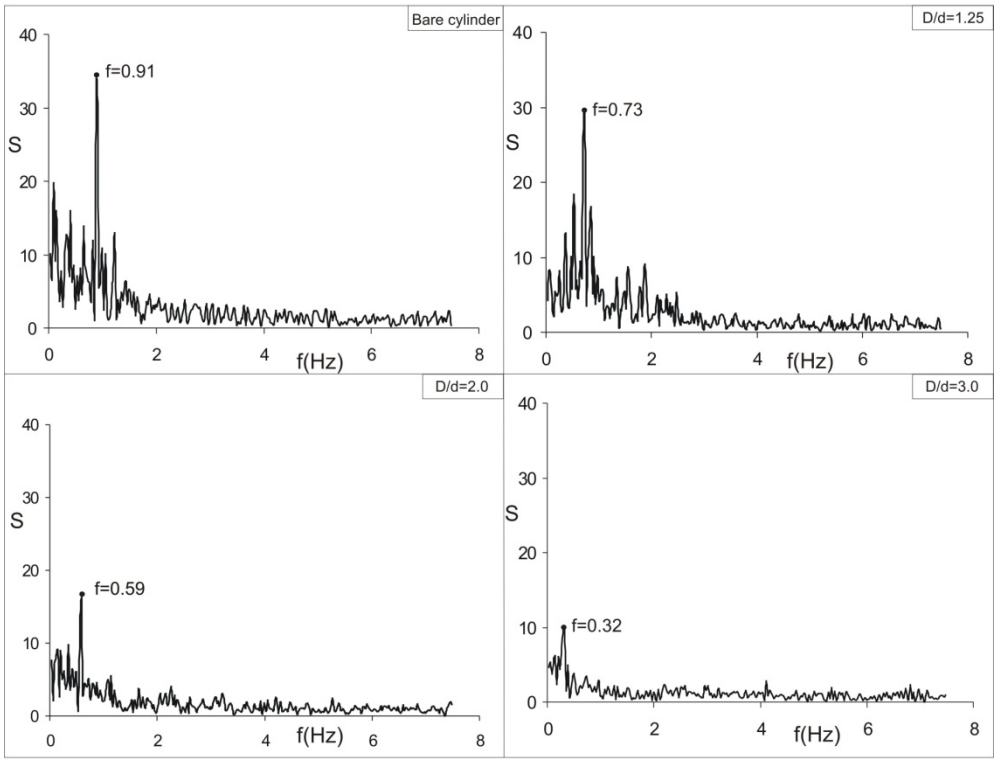

Fig. 6 Comparison of vortex shedding frequencies with varying diameter ratios at the first flow field of flow

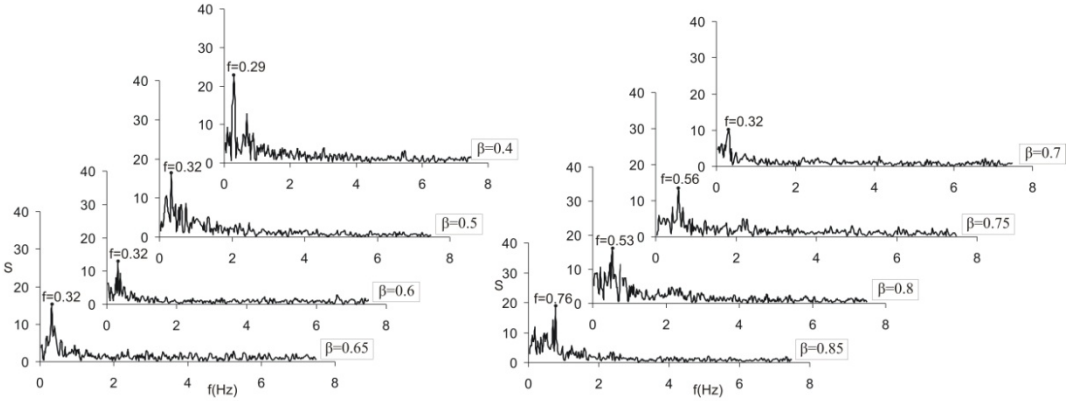

Fig. 7 Spectral analysis of first flow fields for all porosities of D/d=3.0

The spectra of streamwise velocity for the diameter ratio of D/d=3.0 at various porosities are addressed in Fig. 7. It can be concluded from this figure that the porosity plays an important role on the control of unsteady vortex structure downstream of the inner cylinder. For the porosities lower than 0.75 ($\beta<0.75$), the peak value occurs at the frequency of approximately f=0.32 Hz which is nearly 30% of that of bare cylinder case. In the range of $0.4\leq \beta \leq 0.75$, a distinctive change does not occur in the dominant frequency. In contrast to the dominant frequency, the spectral amplitude of the dominant frequency is distinctly attenuated with increasing porosity. In terms of $\beta\geq 0.75$, the dominant frequency increases in comparison with the porosity values of $\beta < 0.75$ as a result of the increase in the open area of the outer permeable cylinder. Therefore, it can be mentioned that bigger porosities ($\beta\geq 0.75$) are less effective on the control of unsteady flow characteristics. As the porosity increases from 0.75 to 0.85, the spectral amplitude of the frequency gradually gets larger due to the higher rate fluctuations originating from the inner -outer cylinders arrangement. Nevertheless, the dominant frequency is less than that of the bare cylinder case.

4. Conclusions

This investigation focused on the control of the flow around a circular cylinder surrounded by outer permeable cylinder in deep water. In order to the explain the flow structure downstream of the cylinder arrangement, the time-averaged patterns of Reynolds shear stress, streamwise velocity contours and turbulent statistics obtained from the PIV measurement have been used. The results depict that both the porosity and the diameter ratio D/d are the parameters which play important role on the suppression of vortex sheeding downstream of the cylinder arrangement. The outer permeable cylinder reduces the wake instabilities and vortex shedding around the cylinder arrangement depending on the porosity and the diameter ratio. The peak values of turbulent quantities, such as Reynolds shear stress and TKE decrease remarkably with increasing the diameter ratio D/d. The spectral analysis of vortex shedding frequency displays that the dominant frequency of vortex shedding downstream of the cylinder arrangement also reduces gradually due

to the weakened Karman shear layer instability. The diameter ratio of D/d=1.25 can not be effective on the attenuation of vortex shedding due to the insufficient gap between the inner and outer cylinders. For this case, it can be concluded that the outer permeable cylinder and the inner cylinder act like a whole cylinder having a diameter of 37.5 mm. On the other hand, the diameter ratio of D/d=3.0 is the most effective one relative to the other diameter ratios. In terms of the porosity, the effectiveness of the porosity of β=0.4 on the suppression of the large scale vortices is less than those of the other porosities. The open area on the surface of the permeable cylinder is too narrow to let the flow in order to penetrate into the wake region. For the range of $0.5 \leq \beta \leq 0.7$, the effect of the permeable cylinder increases progressively with an increase in the porosity and the permeable cylinder yields a decrease by about 70% of the turbulent statistics. This drastic reduction is obtained from β=0.7 case. The present results could be a sign of drag reduction on the inner cylinder. In order to verify these observations and understand the details of flow structure, forthcoming works would concentrate on the measurement of lift and drag forces.

References

Akilli, H., Sahin, B. and Tumen, N.F. (2005), "Suppression of vortex shedding of circular cylinder in shallow water by a splitter plate", *Flow Meas. Instrum.*, **16**(4), 211-219.

Akilli, H., Karakus, C., Akar, A., Sahin, B. and Tumen, N.F. (2008), "Control of vortex shedding of circular cylinder in shallow water flow using an attached splitter plate", *J. Fluid Eng. - T ASME*, **130**(4), 1-11.

Akansu, Y.E. and Fırat, E. (2010), "Control of flow around a square prism by slot jet injection from the rear surface", *Exp. Therm. Fluid Sci.*, **34**(7), 906-914.

Bhattacharyya, S., Dhinakaran, S. and Khalili, A. (2006), "Fluid motion around and through a porous cylinder", *Chem. Eng. Sci.*, **61**(13), 4451-4461.

Bruneau, C.H. and Mortazavi, I. (2006), "Control of vortex shedding around a pipe section using a porous sheath", *Int. J. Offshore Polar.*, **16**(2), 1-7.

Bhattacharyya, S. and Singh, A.K. (2011), "Reduction in drag and vortex shedding frequency through porous sheath around a circular cylinder", *Int J. Numer. Meth. Fl.*, **65**(6), 683-698.

Cattafesta, L.N., Garg, S. and Shukla, D. (2001), "Development of piezoelectric actuators for active flow control", *AIAA J.*, **39**(8), 1562-1568.

Choi, H., Jean, W.P. and Kim, J. (2008), "Control of flow over a bluff body", *Annu. Rev. Fluid Mech.*, **40**, 113-139.

Dol1, S.S., Kopp, G.A. and Martinuzzi, R.J. (2008), "The suppression of periodic vortex shedding from a rotating circular cylinder", *J. Wind Eng. Ind. Aerod.*, **96**(6-7), 1164-1184.

Ekmekci, A. and Rockwell, D. (2010), "Effects of a geometrical surface disturbance on flow past a circular cylinder: a large-scale spanwise wire", *J. Fluid Mech.*, **665**, 120-157.

Feng, L.H. and Wang, J.J. (2010), "Circular cylinder vortex-synchronization control with a synthetic jet positioned at the rear stagnation point", *J. Fluid Mech.*, **662**, 232-259.

Fransson, J.H.M., Konieczny, P. and Alfredsson, P.H. (2004), "Flow around a porous cylinder subject to continuous suction or blowing", *J. Fluid Struct.*, **19**(8), 1031-1048.

Gad El Hak, M. (2007), *Flow control: passive, active and reactive flow*, Cambridge University Press, Cambridge, England.

Gerrard, JH. (1966), "The mechanics of the formation region of vortices behind bluff bodies", *J. Fluid Mech.*, **25**, 401-413.

Gozmen, B., Akilli, H. and Sahin, B. (2013), "Passive control of circular cylinder wake in shallow flow", *Measurement*, **46**(3), 1125-1136.

Kleissl, K. and Georgakis, C.T. (2011), "Aerodynamic control of bridge cables through shape modification: A preliminary study", *J. Fluid Struct.*, **27**(7), 1006-1020.

Kuo, C.H. and Chen, C.C. (2009), "Passive control of wake flow by two small control cylinders at Reynolds number 80", *J. Fluid Struct*., **25**(6), 1021-1028.
Lee, S.J., Lee, S.I. and Park, C.W. (2004), "Reducing the drag on a circular cylinder by upstream installation of a small control rod", *Fluid Dyn. Res*., **34**(4), 233-250.
Lee, S.J. and Lee, J.Y. (2008), "Piv measurements of the wake behind a rotationally oscillating circular cylinder", *J. Fluid Struct*., **24**(1), 2-17.
Lee, T. and Ko, L.S. (2009), "PIV investigation of flowfield behind perforated Gurney-type flaps", *Exp. Fluids*, **46**(6), 1005-1019.
Li, Z., Navon, I.M., Hussaini, M.Y. and Le Dimet, F.X. (2003), "Optimal control of cylinder wakes via suction and blowing", *Comput. Fluids*, **32**(2), 149-171.
Lim, H.C. and Lee, S.J. (2004), "Flow control of a circular cylinder with O-rings", *Fluid Dyn. Res*., **35**(2), 107-122.
Min, C. and Choi, H. (1999), "Suboptimal feedback control of vortex shedding at low Reynolds number", *J. Fluid Mech*., **401**, 123-156.
Nakamura, Y. (1996), "Vortex shedding from bluff bodies with splitter plates", *J. Fluid Struct*., **10**(2), 147-158.
Nakamura, H. and Igarshi, T. (2008), "Omnidirectional reductions in drag and fluctuating forces for a circular cylinder by attaching rings", *J. Wind Eng. Ind. Aerod*., **96**(6-7), 887-899.
Ozgoren, M., Pinar, E., Sahin, B. and Akilli, H. (2011), "Comparison of flow structures in the downstream region of a cylinder and sphere", *Int. J. Heat Fluid Fl*., **32**(6), 1138-1146.
Ozkan, G.M., Oruc, V., Akilli, H. and Sahin, B. (2012), "Flow around a cylinder surrounded by a permeable cylinder in shallow water", *Exp. Fluids*, **53**(6), 1751-1763.
Pinar, E., Ozkan, G.M., Akilli, H. and Sahin, B. (2011), "Flow control downstream of a circular cylinder via a surrounding perforated cylinder", *Proceeding of the 6th Ankara International Aerospace Conference METU*, Ankara, TURKEY, September.
Raffel, M., Willert, C.E. and Kompenhans, J. (1998), *Particle image velocimetry a practical guide*, Springer, Göttingen.
Sobera, M.P., Kleijn, C.R. and Van den Akker, H.E.A. (2006), "Subcritical flow past a circular cylinder surrounded by a porous layer", *Phys. Fluids*, **18**(3), 038106.
Thompson, M., Hourigan, K. and Sheridan, J. (1996), "Three-dimensional Instabilities in the wake of a circular cylinder", *Exp. Therm. Fluid Sci*., **12**(2), 190-196.
Unal, M.F. and Rockwell, D. (1988), "On vortex formation from a cylinder. Part 1: control by splitter-plate interference", *J. Fluid Mech*., **190**, 513-529.
Wang, J.J., Zhang, P.F., Lu, S.F. and Wu, K. (2006), "Drag reduction of a circular cylinder using an upstream rod", *Flow Turbul. Combust*., **76**(1), 83-101.
Willimson, C.H.K. (1996), "Vortex dynamics in the cylinder wake", *Annu. Rev. Fluid. Mech*., **28**, 477-539.
Yucel, S.B., Cetiner, O. and Unal, M.F. (2010), "Interaction of circular cylinder wake with a short asymmetrically located downstream plate", *Exp Fluids*, **49**(1), 241-255.

CC